Journal of Sound and Vibration (2002) **253**(4), 889–908
doi:10.1006/jsvi.2001.4073, available online at http://www.idealibrary.com on IDEAL®

A HIGH-FREQUENCY THREE-DIMENSIONAL TYRE MODEL BASED ON TWO COUPLED ELASTIC LAYERS

K. Larsson and W. Kropp

Department of Applied Acoustics, Chalmers University of Technology, SE-412 96 Göteborg, Sweden.
E-mail: kl@ta.chalmers.se

(*Received* 9 *December* 1999, *and in final form* 3 *October* 2001)

Road traffic noise is today a serious environmental problem in urban areas. The dominating noise source at speeds greater than 50 km/h is car tyres. In order to achieve a reduction of traffic noise tyres have to become quieter. To reduce tyre/road noise a deep understanding of the noise generation mechanisms is of major importance. An existing tyre/road noise simulation model consists of a smooth tyre rolling at a constant speed on a rough road surface. It is composed of three separate modules: a tyre model, a contact model and a radiation model. The major drawback with the contact model is that it only takes the radial component of the contact forces into account. To improve this model, a description of the tangential motion at high frequencies is necessary. Most of the models for the structure-borne sound behaviour of tyres are designed for the low-frequency range (i.e., below 400 Hz). Above this frequency range, the curvature of the tyre is unimportant, while the internal structure (multi-layers of steel and rubber) increases in importance. For the high-frequency range, a double-layer tyre model is proposed, which is based on the general field equations, to take into account the tangential motion and the local deformation of the tread. Both propagating waves and mode shapes have been investigated by the use of this model. Calculations of the response of the tyre to an external excitation show relatively good agreement with measurements on a smooth tyre.

1. INTRODUCTION

1.1. BACKGROUND

Today noise is considered as one of the largest environmental problems in urban areas in Europe. According to reference [1], 20% of the population is exposed to sound pressure levels greater than 55 dB(A) and more than 65% to levels greater than 55 dB(A) outside their windows. This level does not constitute a good sound environment. The major part of the environmental noise comes from road traffic.

Tyre/road noise is the dominant noise source for vehicles at driving speeds greater than 30–50 km/h. During the last 20 years, research has focused on reduction of the noise generated by the engine, exhaust system and transmission line in vehicles. The tyres, however, are said to be as noisy today as 20 years ago [2]. Tyre/road noise is today the limiting factor for the reduction of road traffic noise. Further reductions of the noise from engine, exhaust system, transmission line, etc. are less and less noticeable in the form of a reduction of the environmental noise.

0022-460X/02/$35.00

1.2. RESEARCH ON TYRE/ROAD NOISE

To be able to reduce the noise from tyres a deep understanding of the noise generation mechanisms involved in the interaction between the tyre and the road surface is of major importance. Basically, two different mechanisms can be observed [3]:

- *Vibrations of the tyre*. The time-varying contact forces will cause vibrations of the tyre, which will radiate sound.
- *The air resonance phenomenon*. For example, the grooves of the pattern will act as Helmholtz resonators, and the air is pushed out of the contact area in front of the tyre and sucked into the contact at the trailing edge, the so-called air pumping effect.

An additional noise source not included in either of these two classes is the local deformation of the tread. The rubber in the tread is, compared to the road surface, very soft with a low shear modulus and a high Poisson ratio. Small roughness peaks in the road surface will cause a local deformation in the tread around the peak when it comes into contact with the tyre. This effect was investigated by Ronneberger [4] and was shown to be a possible noise source at medium and high frequencies.

Previously, a complete simulation model for tyre/road noise prediction has been developed [5], consisting of a smooth tyre rolling at constant speed over a rough road surface. This simulation model is composed of three modules, namely

- A tyre model, where the dynamic properties of a tyre are considered.
- A contact model, where the non-linear contact forces during the rolling process and the resulting vibration velocities on the tyre are calculated.
- A radiation model, where the sound radiation from the tyre due to the velocity field on the tyre is calculated.

One major drawback of this simulation model is the contact model where only the radial part of the contact forces is taken into account. In reality, there are also tangential and lateral forces acting in the contact zone. The tangential forces originate mainly from three mechanisms:

1. Geometry, the tread blocks enter the contact zone at an angle relative to the road. The resulting force can be divided into one radial and one tangential component.
2. Friction, due to the velocity differences between the vibrating tyre and the road surface, time-varying tangential friction forces will act on the tread.
3. Roughness, the roughness of the road surface leads to a variation of the radial contact forces, which in turn affect the tangential friction forces.

In order to improve the contact model the dynamic tyre model has to be able to include the reaction to both radial and tangential contact forces.

1.3. EXISTING TYRE MODELS

A lot of research on the vibrational properties of vehicle tyres has been done during the last decades.

One of the first tyre models was the circular ring model developed by Böhm [6]. The model takes radial, tangential as well as lateral motions into account. Pacejka [7] modelled the tyre belt as a circular beam under tension, supported by an elastic bedding. The model is similar to the circular ring model by Böhm, but no lateral motion is included in the model. He also developed models for the lateral vibrations, where the tyre was modelled as one or

several strings [8]. Padovan [9] included the viscoelastic effects, both for the belt and for the foundation in the circular ring model. These models are valid as long as the wavelength is large compared to the width of the tyre, which typically is below 400 Hz.

A number of examples where the finite element method has been applied to tyres can be found in the literature, for example, references [10–12].

At frequencies above the ring frequency, the curvature of the tyre can be disregarded. The radial and the tangential motions can be considered as uncoupled. To model the vibrational tyre properties in this frequency range, Kropp [13] proposed the orthotropic plate model, where the tyre belt is modelled as a finite plate, having different properties in tangential and lateral directions. Uebler [14] developed a model where the belt and the side walls were modelled as a set of individual Mindlin plates coupled together to represent the curvature in the lateral direction. Pinnington *et al.* [15] suggested the tyre to be modelled as an infinite Timoshenko beam with waves propagating along the tyre, taking shear and rotational effects into account.

None of the tyre models found in the literature is appropriate for the modelling of radial and tangential vibrations at high frequencies including the local deformation. This motivates the development of an improved high-frequency tyre model including these effects.

In the following, a tyre model including the tangential motion and the local deformation will be derived. Results will be shown in the form of dispersion relations for the wave types in the frequency range of interest, wave speeds for this model compared to wave speeds both calculated by previous models and measurements and driving point mobilities in radial and tangential directions compared to measurements.

2. PRESENT MODEL

A model for the description of the structure-borne sound propagation of a tyre has been developed. A tyre is a complex structure composed of comparatively stiff belts, made of several layers of steel-reinforced rubber, and a tread layer, made of soft rubber, see Figure 1.

The steel threads in the stiff belt have different orientations in order to give proper mechanical characteristics. The complex structure makes it difficult, if not impossible, to

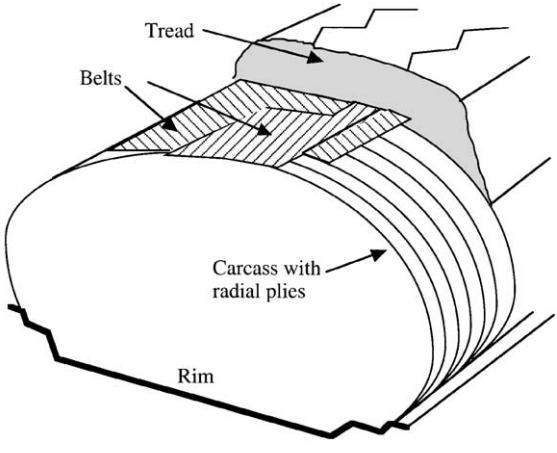

Figure 1. Internal structure of a radial ply, belted tyre. The belts are made of differently orientated threads in a rubber matrix. The tread is made of soft rubber.

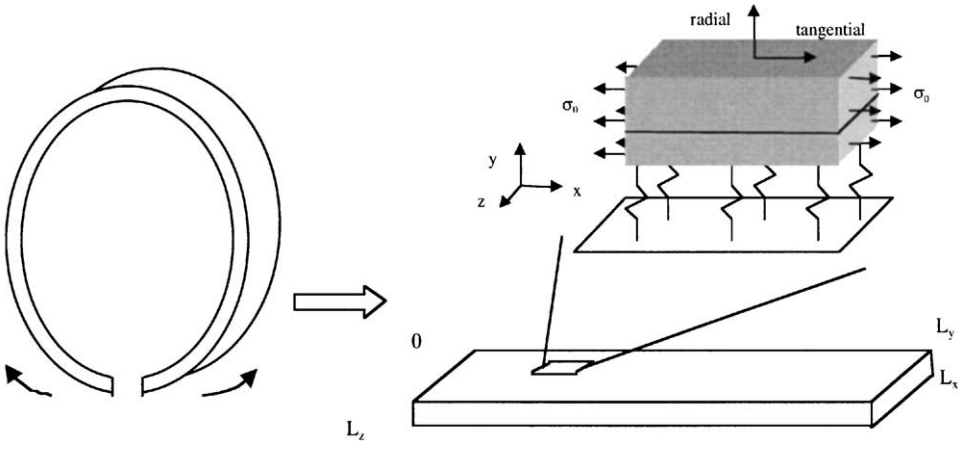

Figure 2. A plate represents the unfolded tyre above the ring frquency. The tyre model is constituted by two coupled elastic layers under tension on an elastic bedding. The bedding consists of individual springs in the x (tangential), y (radial), and z (lateral) directions.

model the tyre analytically without making a number of simplifications. At high frequencies (above 400 Hz, which is the ring frequency), the curvature of the tyre may be neglected, while the internal structure increases in importance. Additionally, the thickness of the tread layer is no longer thin compared to the wavelength at frequencies above 2 kHz. The model presented here consists of a double-layered isotropic thick plate under tension. Two elastic layers having different thicknesses and material properties are coupled together. The bottom layer represents the stiff belt, while the top layer represents the soft rubber surface. To take into account the effects of the side walls and the air inside the tyre, an elastic bedding supports the plate in the radial, tangential and lateral directions. The model is shown in Figure 2. Using this model, the propagation of free waves for an infinite plate are studied and compared to dispersion relations using other tyre models and measurements. Additionally, the response of the plate to external excitations in the radial and tangential directions is calculated and compared to measurements.

2.1. MATHEMATICAL MODEL

To study the deformations of an elastic layer subjected to an external tension, the general field equations (GFE) are derived by the use of Hamilton's principle, as nicely demonstrated by Heckl, see references [16, 17]. This is a very convenient method to use for complicated systems, since the only expressions needed in the formulation are the kinetic and the potential energies of the system. Hamilton's principle is given in equation (1), where W_{kin} is the kinetic energy, W_{pot} is the potential energy and δ is the variation operation.

$$\delta \int (W_{kin} - W_{pot})\, \mathrm{d}t = 0. \tag{1}$$

2.1.1. *Kinetic energy*

The deformation of a point in the solid is given as the deformation vector $\mathbf{u}$ in equation (2).

$$\mathbf{u} = (\xi(x, y, z, t), \eta(x, y, z, t), \zeta(x, y, z, t)). \tag{2}$$

The total kinetic energy of a solid body under deformation is given in equation (3), where ρ is the density of the material and the integration is performed over the volume, V, of the solid:

$$W_{kin} = \int_V \frac{1}{2}\rho\left[\left(\frac{\partial\xi}{\partial t}\right)^2 + \left(\frac{\partial\eta}{\partial t}\right)^2 + \left(\frac{\partial\zeta}{\partial t}\right)^2\right]\mathrm{d}V. \tag{3}$$

2.1.2. *Potential energy*

The potential energy in the layer during the deformation originates from two kinds of mechanisms:

- The elastic deformation energy from the strain during the displacements.
- The external tension gives an additional contribution to the potential energy similar to a stretched vibrating string.

Elastic deformation. The part of the potential energy coming from the linear elastic deformation of the material can be formulated according to

$$W_{pot}^{elastic} = \int_V \sigma_{i,j}\,\varepsilon_{i,j}\,\mathrm{d}V, \tag{4}$$

where $i, j = x, y, z$.

In equation (4) the stresses are assumed to follow Hooke's law for a linear isotropic material, according to

$$\sigma_{i,j} = 2G\left(\frac{v}{1-2v}\varepsilon_{k,k}\delta_{k,k} + \varepsilon_{i,j}\right), \tag{5}$$

where the strains are defined as

$$\varepsilon_{i,j} = \frac{1}{2}\left(\frac{\partial u_i}{\partial x_j} + \frac{\partial u_j}{\partial x_i}\right).$$

In the equations the summation convention is used (summation over repeated indexes k), and $\delta_{k,k}$ denotes the Kroneckers delta function, G is the shear modulus of the material and v is the Poisson ratio.

External tension: To take into account the external tension acting on the layers, a non-linear strain definition is used, in this case the "finite strain" or "Green–Lagrange" strain tensor [18, 19]. The additional potential energy from the external tension is shown by

$$W_{pot}^{ext} = \int_V \sigma_{i,j}^{ext}\,\varepsilon_{i,j}^{finite}\,\mathrm{d}V, \tag{6}$$

where

$$\varepsilon_{i,j}^{finite} = \frac{1}{2}\left(\frac{\partial u_i}{\partial x_j} + \frac{\partial u_j}{\partial x_i} + \frac{\partial u_k}{\partial x_i}\frac{\partial u_k}{\partial x_j}\right).$$

2.2. THE GENERAL FIELD EQUATIONS

Using equations (3–6) and performing the calculation of the variation according to equation (1) gives the general field equations for a single layer exposed to an external

tension, equation (7). Here the external tension is assumed to be constant, σ_0, and acts only in the x (tangential) direction. Since at low frequencies (i.e., below about 400 Hz) the tyre can be considered as a beam, disregarding a tension in the lateral direction can be justified. At frequencies where the wave propagation also takes place in the lateral direction (above approximately 400 Hz), the tensional waves are of minor importance, and the wave field is dominated by bending waves. These assumptions, are verified by the study of the dispersion relations as well as by comparisons of the results with measurements of the point mobility.

$$\begin{aligned}
G\left[\Delta\xi + \frac{1}{1-2\nu}\frac{\partial}{\partial x}(\nabla\cdot\mathbf{u})\right] + \sigma_0\frac{\partial^2\xi}{\partial x^2} &= \rho\frac{\partial^2\xi}{\partial t^2},\\
G\left[\Delta\eta + \frac{1}{1-2\nu}\frac{\partial}{\partial y}(\nabla\cdot\mathbf{u})\right] + \sigma_0\frac{\partial^2\eta}{\partial x^2} &= \rho\frac{\partial^2\eta}{\partial t^2},\\
G\left[\Delta\zeta + \frac{1}{1-2\nu}\frac{\partial}{\partial z}(\nabla\cdot\mathbf{u})\right] + \sigma_0\frac{\partial^2\zeta}{\partial x^2} &= \rho\frac{\partial^2\zeta}{\partial t^2},
\end{aligned} \tag{7}$$

where Δ is the Laplace operator and ∇ is the nabla operator.

Equation (7) has been formulated without taking into account the external tension in many textbooks (e.g., reference [17]). It can be interesting to note that the classical string equation appears in equation (7).

3. SOLUTIONS TO THE HOMOGENEOUS EQUATIONS

The general field equations can be solved by the use of a Fourier transformation technique. The unknown variables are transformed into the frequency–wave number domain from the original time–space domain. The transformation into the wave number domain is given in equation (8), where k_1, k_2, and k_3 are the wave numbers in the x, y, and z directions respectively. Harmonic motion is assumed, and the common factor $\mathrm{e}^{\mathrm{j}\omega t}$ is omitted in the following.

$$\begin{aligned}
\xi &= \frac{1}{(2\pi)^3}\int_{-\infty}^{\infty}\hat{\xi}\,\mathrm{e}^{-\mathrm{j}k_1x}\mathrm{e}^{-\mathrm{j}k_2y}\mathrm{e}^{-\mathrm{j}k_3z}\,\mathrm{d}k_1\,\mathrm{d}k_2\,\mathrm{d}k_3,\\
\eta &= \frac{1}{(2\pi)^3}\int_{-\infty}^{\infty}\hat{\eta}\,\mathrm{e}^{-\mathrm{j}k_1x}\mathrm{e}^{-\mathrm{j}k_2y}\mathrm{e}^{-\mathrm{j}k_3z}\,\mathrm{d}k_1\,\mathrm{d}k_2\,\mathrm{d}k_3,\\
\zeta &= \frac{1}{(2\pi)^3}\int_{-\infty}^{\infty}\hat{\zeta}\,\mathrm{e}^{-\mathrm{j}k_1x}\mathrm{e}^{-\mathrm{j}k_2y}\mathrm{e}^{-\mathrm{j}k_3z}\,\mathrm{d}k_1\,\mathrm{d}k_2\,\mathrm{d}k_3.
\end{aligned} \tag{8}$$

These expressions are introduced into the GFE, transforming the coupled partial differential equation system into a system of linear algebraic equations in the new variables. The equation system can be written in a matrix formulation and solved by the use of standard linear algebra. The matrix formulation of the GFE is shown by

$$\begin{pmatrix} m_{11} & m_{12} & m_{13}\\ m_{21} & m_{22} & m_{23}\\ m_{31} & m_{32} & m_{33}\end{pmatrix}\begin{pmatrix}\hat{\xi}\\ \hat{\eta}\\ \hat{\zeta}\end{pmatrix} = k_s^2\begin{pmatrix}\hat{\xi}\\ \hat{\eta}\\ \hat{\zeta}\end{pmatrix}, \tag{9}$$

where

$$m_{11} = (1 + a + c)k_1^2 + k_2^2 + k_3^2, \quad m_{21} = m_{12}, \quad m_{31} = m_{13},$$

$$m_{12} = ak_1k_2, \quad m_{22} = (1 + c)k_1^2 + (1 + a)k_2^2 + k_3^2, \quad m_{32} = m_{23},$$

$$m_{13} = ak_1k_3, \quad m_{23} = ak_2k_3, \quad m_{33} = (1 + c)k_1^2 + k_2^2 + (1 + a)k_3^2$$

$$a = \frac{1}{1 - 2v}, \qquad c = \frac{\sigma_0}{G}, \qquad k_s^2 = \omega^2 \frac{\rho}{G}.$$

The non-trivial solutions to equation (9) can be found from the eigenvalues and the eigenvectors for the matrix, which have been calculated analytically. The results for the eigenvalues are given in equations (10) and (11), while the three eigenvectors are given in equation (12).

$$\lambda_{1,2} = k_{s,1,2}^2 = (1 + c)k_1^2 + k_2^2 + k_3^2, \tag{10}$$

$$\lambda_3 = k_{s,3}^2 = (1 + a + c)k_1^2 + (1 + a)(k_2^2 + k_3^2), \tag{11}$$

$$\mathbf{v}_1 = \begin{pmatrix} \hat{\xi} \\ \hat{\eta} \\ \hat{\zeta} \end{pmatrix} = \begin{pmatrix} k_3 \\ 0 \\ -k_1 \end{pmatrix}, \quad \mathbf{v}_2 = \begin{pmatrix} k_2 \\ -k_1 \\ 0 \end{pmatrix}, \quad \mathbf{v}_3 = \begin{pmatrix} k_1 \\ k_2 \\ k_3 \end{pmatrix}. \tag{12}$$

The eigenvalues give the relations between the wave numbers in different directions and frequency, while the eigenvectors give the relative amplitudes in the different directions of the wave. These results show that two different wave types are present in the solid. The first two identical eigenvalues correspond to transversal waves, where the displacements are perpendicular to the direction of propagation. The third eigenvalue corresponds to pure longitudinal waves, where the displacements are parallel to the direction of propagation. The transversal wave can be divided into two orthogonal polarized waves, where only the first one has displacements in the horizontal plane (x–z), while the second one only deforms in the vertical (x–z) plane. The two transversal waves are often referred to as rotational or horizontally and vertically polarized S (secondary) waves in the literature, while the pure longitudinal wave is cited as an irrotational or as a P (primary) wave [20]. The eigenvalues in this case become identical with the ones found for a solid without any external tension if c is assumed to be zero in equations (10) and (11). The eigenvectors, equation (12), are identical to the eigenvectors found without external tension.

Equations (10) and (11) (the eigenvalues) give restrictions on which wave numbers are possible for plane waves in the solid for a specific frequency, while equation (12) (the eigenvectors) gives the relative amplitude ratios for each wave. In this way the number of unknowns is reduced. When the frequency is determined, i.e., k_s, and the plate is considered as infinite in the x and z directions, the wave number in the thickness of the tyre is defined, which is given by

$$q_1 = q_2 = k_2 = \pm \sqrt{k_s^2 - (1 + c)k_1^2 - k_3^2}, \tag{13}$$

$$q_3 = k_2 = \pm \sqrt{\frac{k_s^2 - (1 + a + c)k_1^2 - (1 + a)k_3^2}{(1 + a)}}. \tag{14}$$

The displacements inside the solid can in this way be written as a sum over the three plane wave types travelling in the positive and negative y directions according to

$$\xi = \int_{-\infty}^{\infty} \sum_{n=1}^{3} \left[(A_{n+} \mathrm{e}^{-\mathrm{j}q_n y} + A_{n-} \mathrm{e}^{\mathrm{j}q_n y}) \boldsymbol{v}_n(\hat{\xi}) \right] \mathrm{e}^{-\mathrm{j}k_1 x} \mathrm{e}^{-\mathrm{j}k_3 z} \, \mathrm{d}k_1 \, \mathrm{d}k_3,$$

$$\eta = \int_{-\infty}^{\infty} \sum_{n=1}^{3} \left[(A_{n+} \mathrm{e}^{-\mathrm{j}q_n y} + A_{n-} \mathrm{e}^{\mathrm{j}q_n y}) \boldsymbol{v}_n(\hat{\eta}) \right] \mathrm{e}^{-\mathrm{j}k_1 x} \mathrm{e}^{-\mathrm{j}k_3 z} \, \mathrm{d}k_1 \, \mathrm{d}k_3, \tag{15}$$

$$\zeta = \int_{-\infty}^{\infty} \sum_{n=1}^{3} \left[(A_{n+} \mathrm{e}^{-\mathrm{j}q_n y} + A_{n-} \mathrm{e}^{\mathrm{j}q_n y}) \boldsymbol{v}_n(\hat{\zeta}) \right] \mathrm{e}^{-\mathrm{j}k_1 x} \mathrm{e}^{-\mathrm{j}k_3 z} \, \mathrm{d}k_1 \, \mathrm{d}k_3,$$

where $\boldsymbol{v}_n(\hat{\xi})$, $\boldsymbol{v}_n(\hat{\eta})$, $\boldsymbol{v}_n(\hat{\zeta})$ are the amplitude ratios, i.e., the components of the eigenvectors in x, y and z directions, respectively, and A_{n+}, A_{n-} are the unknown amplitudes.

This means that six unknown amplitudes have to be solved for each layer. Equation (15) can be interpreted as the displacement field which is expressed as the projections of the eigenvectors along the y-axis propagating in x and z directions.

3.1. COUPLING OF THE LAYERS, BOUNDARY CONDITIONS

Basically, there are two different ways to study the characteristics of multi-layered structures at high frequencies; the transfer matrix method and the global matrix method [21]. In this analysis, the global matrix method is used exclusively. One benefit with the global matrix method is its stability related to large values of the frequency-thickness product. However, the frequency range of interest in this study does not lead to frequency-thickness products that are problematic from a numerical point of view.

The coupling of the layers is done by introducing boundary conditions, which are fulfilled for the complete multi-layered plate. The boundary conditions are given at each side of each layer, and a global matrix is assembled containing the coupled equations. The stresses at all surfaces and interfaces are given as boundary conditions, as well as the displacements at the interfaces of the layers. In the case considered, the stresses and displacements at the interfaces are assumed to be equal in the two connected layers, which means that the layers are perfectly bonded, i.e. no slip occurs at the interfaces. At the bottom layer the stresses are assumed to be identical to the stresses induced by the bedding. At the free top surface all the stresses have to vanish.

The stresses are assumed to follow Hooke's law for a linear, isotropic material and are given in equation (5).

Since there are six unknown amplitudes in each layer, twelve equations have to be formulated. The boundary conditions of interest in this case is given by

$$\begin{aligned}
&\sigma_{yy}^{lay1}(y=0) = s_y \eta^{lay1}(y=0), && \xi^{lay1}(y=h_1) = \xi^{lay2}(y=h_1),\\
&\sigma_{yx}^{lay1}(y=0) = s_x \xi^{lay1}(y=0), && \eta^{lay1}(y=h_1) = \eta^{lay2}(y=h_1),\\
&\sigma_{yz}^{lay1}(y=0) = s_z \zeta^{lay1}(y=0), && \zeta^{lay1}(y=h_1) = \zeta^{lay2}(y=h_1),\\
&\sigma_{yy}^{lay1}(y=h_1) = \sigma_{yy}^{lay2}(y=h_1), && \sigma_{yy}^{lay2}(y=h_2) = 0,\\
&\sigma_{yx}^{lay1}(y=h_1) = \sigma_{yx}^{lay2}(y=h_1), && \sigma_{yx}^{lay2}(y=h_2) = 0,\\
&\sigma_{yz}^{lay1}(y=h_1) = \sigma_{yz}^{lay2}(y=h_1), && \sigma_{yz}^{lay2}(y=h_2) = 0.
\end{aligned} \tag{16}$$

Inserting the expressions for the stresses, see equation (5), and displacements, see equation (15), gives the global 12×12 matrix equation as shown in

$$\begin{pmatrix} b_{1,1} & b_{1,2} & \cdots & b_{1,12} \\ b_{2,1} & b_{2,2} & & \\ \vdots & & \ddots & \vdots \\ b_{12,1} & & \cdots & b_{12,12} \end{pmatrix} \begin{pmatrix} A_{1+}^{lay1} \\ A_{1-}^{lay1} \\ A_{2+}^{lay1} \\ A_{2-}^{lay1} \\ A_{3+}^{lay1} \\ A_{3-}^{lay1} \\ A_{1+}^{lay2} \\ A_{1-}^{lay2} \\ A_{2+}^{lay2} \\ A_{2-}^{lay2} \\ A_{3+}^{lay2} \\ A_{3-}^{lay2} \end{pmatrix} = 0, \tag{17}$$

OT in matrix form $\mathbf{B} \cdot \mathbf{A} = \mathbf{0}$. Non-trivial solutions to the boundary condition equations imply that the determinant of the global matrix $\mathbf{B}$ has to be equal to zero.

3.2. FREELY PROPAGATING WAVES

Due to the high damping in the rubber material at high frequencies, the tyre might be considered as an infinite waveguide, where waves are propagating along the tyre circumference. These wave types can be studied by the model described above. To find the dispersion relations for free waves travelling along the plate, it is considered as a two-dimensional, infinitely long layer. Putting k_3 to zero and assuming plain strain conditions for the deformation, i.e., only deformations in the x–y plane, gives a new two-dimensional field equation from equation (7). Since the new formulation of the field equation is two dimensional, only two free plane wave types can be found, one transversal wave with deformations in the x–y plane only, and one pure longitudinal wave. The wave field can be seen as a superposition of these two plane waves. The out of plane shear wave is not included in the model due to the plane strain conditions. However, this wave type does not couple to the other wave types and hence, does not influence the results for the two-dimensional model.

3.2.1. *Wave types*

Dispersion relations for the free waves travelling along the tyre at a specific frequency can be found by solving the homogeneous boundary conditions for that frequency. Wave numbers, which give a vanishing determinant of the global matrix formulated from equation (16), correspond to free propagating waves. In the frequency range of interest (i.e., up to 3 kHz), three wave types are found to be important and are shown in Figure 3.

The first wave type is a membrane wave at low frequencies, due to the external tension, and a bending wave at medium frequencies. The second wave type is a longitudinal wave. The last wave type is an in-plane wave where the two layers are moving out of phase relative to each other. This last wave type has been referred to as a rotational wave in the literature, see reference [15].

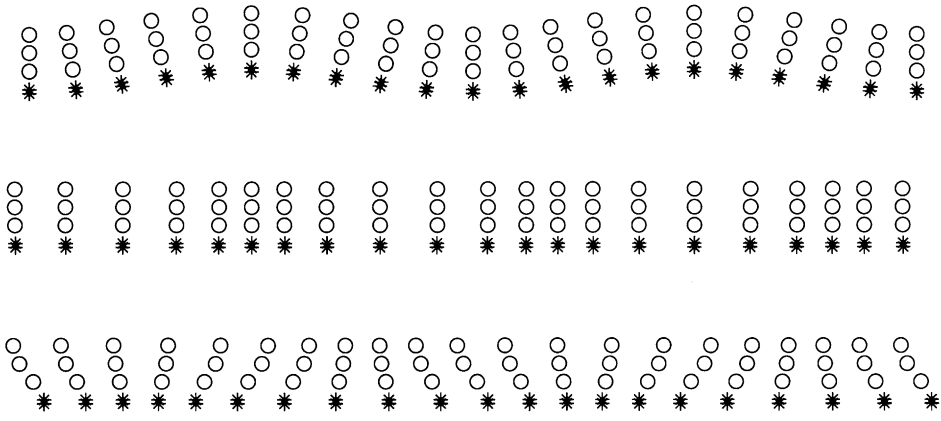

Figure 3. The three wave types considered in the model. Rings represent points in the rubber tread layer and stars represent points in the stiff belt layer.

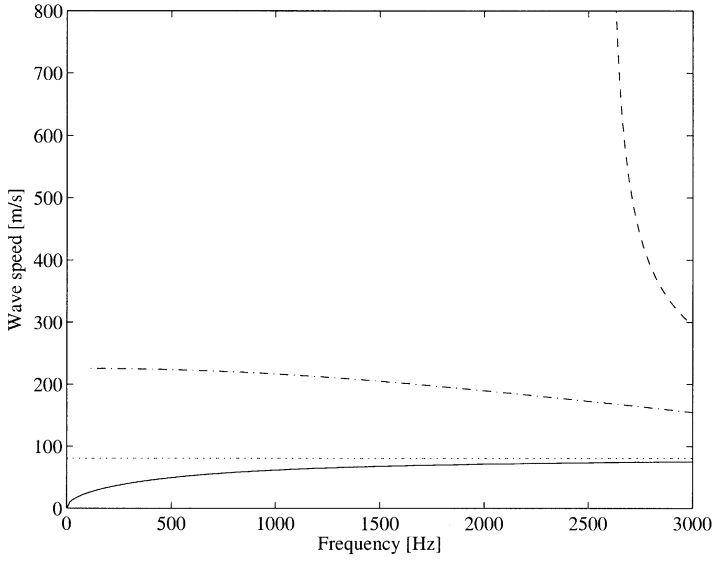

Figure 4. Dispersion relations for the three wave types represented in the model. ——, wave type 1; ·–·–·–·, wave type 2; – – – –, wave type 3; ....., Rayleigh waves in rubber.

3.2.2. *Dispersion relations for the wave types*

Figure 4 shows the dispersion relations for the three waves propagating along the double-layer plate without external tension and bedding. The speed of the waves is plotted as a function of frequency for the bending, longitudinal and the in-plane wave.

In the figure, no membrane effect can be seen for the first wave type, as expected. The dispersion relation for the bending waves is proportional to the square root of the frequency at low frequencies. The speed of the longitudinal waves is constant at low frequencies, but is decreasing at higher frequencies towards the speed of the surface waves (Rayleigh waves) in the rubber material, which is also shown in Figure 4. The speed of the in-plane wave (wave type 3) is very high at the cut-on frequency (about 2500 Hz), but decreases fast to a value

TABLE 1

Material data used in the two-layer model

	Layer 1 (belt)	Layer 2 (tread)
Young's modulus (MPa)	400	20
Density (kg/m^3)	2400	950
Poisson ratio	0·3	0·47
Thickness (mm)	1	14
External tension (MPa)	62·7	0
Bedding stiffness x, y, z, (MN/m^3)	2·85, 8·55,	−2·85

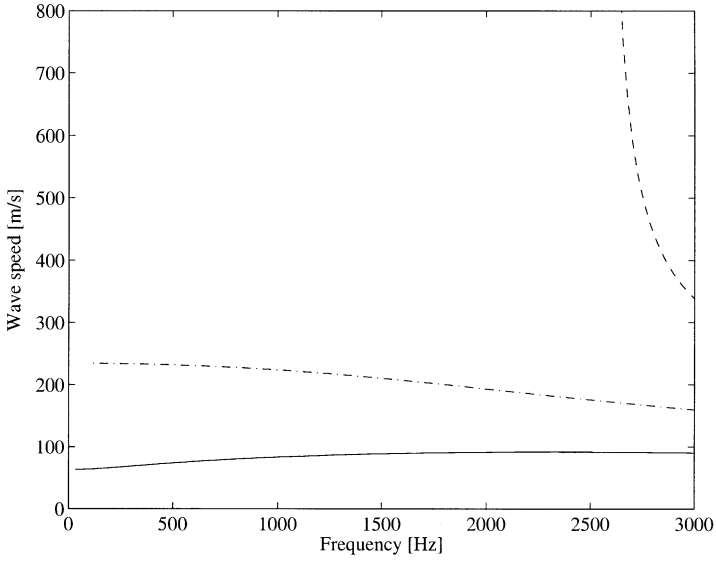

Figure 5. Dispersion relations for waves in the plate subjected to an external tension. ——, wave type 1; ·–·–·–, wave type 2; – – –, wave type 3.

close to that of bending and longitudinal waves. The material data used in the calculations are listed in Table 1.

Influence of external tension: Figure 5 shows the dispersion relation for the three wave types when an external tension is applied to the bottom layer of the plate. In the figure, the membrane effect can be clearly seen in the wave speed for the first wave type at low frequencies.

The speed of wave type 1 is approaching a constant level when the frequency decreases towards zero. This behaviour supports the theory on membrane waves. It can also be seen in the figure that the speed of the second and third wave type is only slightly influenced by the tension.

Influence of bedding: The dispersion relations for the wave types, when the plate is both exposed to an external tension and supported by an elastic bedding, are shown in Figure 6. The radial bedding influences wave type 1 at low frequencies, where the speed of the wave increases rapidly. The tangential bedding influences the longitudinal waves at low frequencies in the same way as the bending waves are affected by the radial bedding. The in-plane waves are not affected at all by the bedding. Since the elastic foundation is

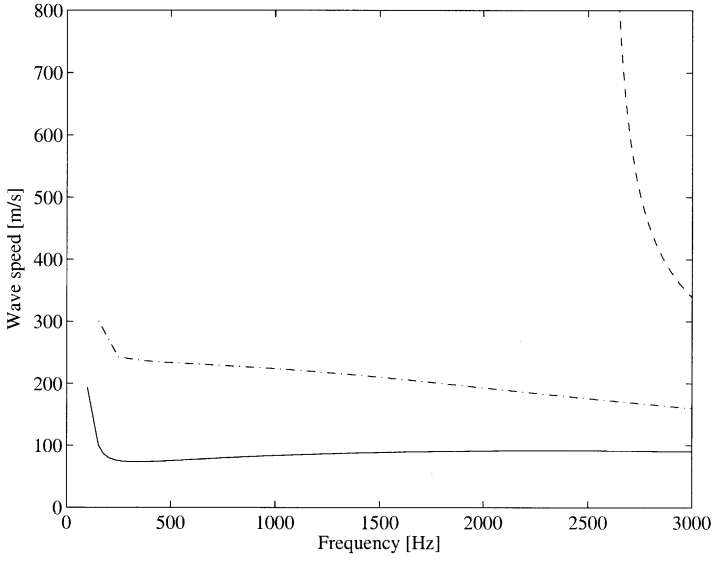

Figure 6. Dispersion relations for waves travelling along a plate subjected to an external tension and supported by a bedding. ——, wave type 1; ·–·–·–, wave type 2; – – –, wave type 3.

modelled by linear springs, the influence from the bedding is visible below and around the resonance frequency of the mass–spring system formed by the plate and the bedding. This means that, for high frequencies, the plate is uncoupled from the rim and that the influence of the side walls and the enclosed air cavity is unimportant for the vibrations of the plate. This effect is also observed in the measured radial driving point mobility of the tyre structure.

3.2.3. *Comparison to the circular ring model*

The circular ring model by Böhm has previously been used to calculate the dispersion relations for the membrane-bending and the longitudinal wave types and compared to measurements on tyres, see e.g., reference [22]. In order to verify the two-layer model a comparison with the ring model has been made, which is shown in Figure 7. In the calculations the material data used for the two-layer model are shown in Table 1.

For the ring model the material data have been expressed to fit to the parameters of the ring, e.g., the bending stiffness and Young's modulus are used instead of the shear modulus and the thickness of the individual layers. The curve of the dispersion relation calculated by the two-layer model has lower resolution than the dispersion relation calculated by the ring model, which is the reason for the "rough" shape of the curve at low frequencies.

The speed of the waves calculated by the use of the two-layer model is decreasing at high frequencies and approaches the speed of the surface waves in the soft tread rubber material. Additionally, the speed of the bending waves, calculated by the circular ring model, approaches infinity as the frequency increases, like bending waves on a beam.

3.2.4. *Comparison with measurements*

Measurements of the dispersion relation for the first wave type (membrane-bending) are available from the work in a master thesis project [23]. There the tyre was excited over the

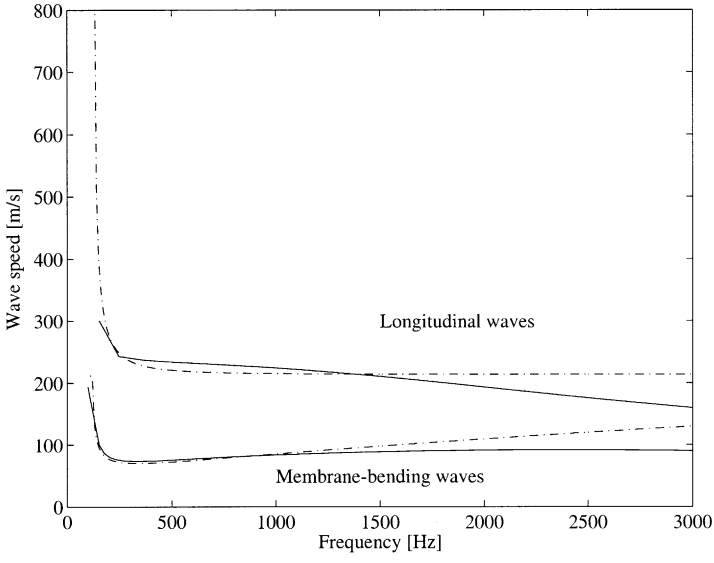

Figure 7. Dispersion relations from the two-layer model compared to the circular ring model. ——, 2-layer model; ·–·–·–, ring model.

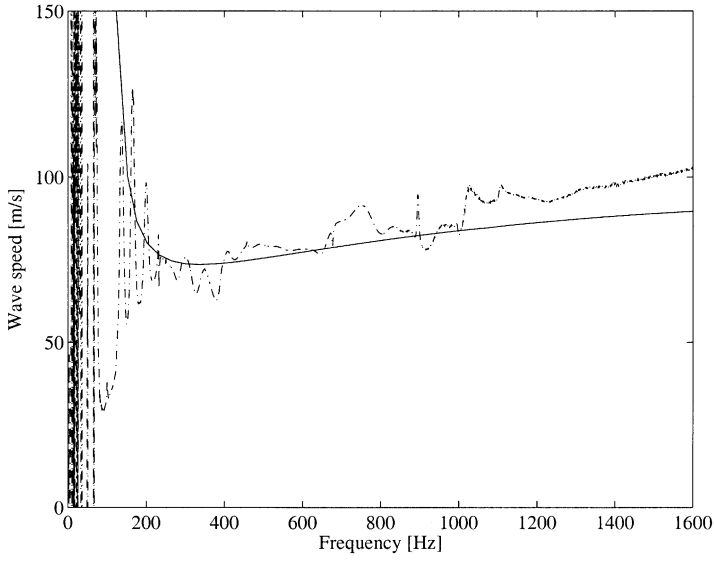

Figure 8. Dispersion relations for membrane-bending waves measured on a tyre and calculated from the two-layer model. ———, calculation; ·–·–·–·, measurement.

whole width of the belt uniformly. Acceleration was measured in two points on the circumference of the tyre and the phase difference between both positions was evaluated in order to obtain the phase speed. This procedure demands that the wave field is propagating, i.e., no standing wave patterns are present on the tyre circumference.

Figure 8 shows a comparison between the calculated wave speed from the two-layer model and measurements on a typical vehicle tyre. The results show good agreement between the two curves, at least at low frequencies and middle frequencies where the tyre vibration is determined by the tension in the belt. The reason for the discrepancy at higher frequencies is the difference in the material data used in the calculations and the real data for the tyre. The material data available in the literature are often given as average values for the complete tyre cross-section, which is very hard to translate to the material parameters needed in the two-layer model. To improve the model, material data would be required to measure separately for each layer, however, this was beyond the scope of this paper.

4. FORCED VIBRATIONS

To calculate the response of the tyre to an external excitation a wave approach method is used, where the external force is considered as a boundary condition on the upper face of the plate. Both the response and the excitation force are Fourier transformed, and the amplitude of the response can be calculated directly at a certain frequency for each wave number.

In the wave approach, the amplitude of a propagating wave is calculated for the actual excitation. The external excitation forces are included in the boundary conditions, instead of in the equations of motion. The twelve boundary condition equations forming an inhomogeneous system can be solved by linear algebra. In order to reduce the calculation effort, symmetry and geometry considerations are used to reduce the number of wave numbers needed for the integration.

The response at a point is given according to equation (8), where the integration has to be performed over all positive and negative wave numbers. The external excitation is in this case seen as a pressure distribution on the top surface of the upper layer, which is Fourier transformed in the same way as the displacements to give a set of linear equations for each wave number.

The plate, representing the unfolded tyre, is seen as simply supported in the width direction along the edges of the rim. These conditions are fulfilled when half of a wavelength fits to the width of the tyre. Since the circular tyre is unfolded, the boundary conditions in the x direction are periodic, see Figure 2. Due to this periodicity in the length direction, the boundary conditions are only fulfilled when a complete wavelength fits to the tyre circumference. Equations (18) and (19) give the possible wave numbers in the length and the width directions respectively.

$$k_1 = 2\pi m/L_x, \quad m = 1,2,3, \ldots , \tag{18}$$

$$k_3 = \pi n/L_z, \quad n = 1,2,3, \ldots . \tag{19}$$

Due to the symmetry of the plate and the excitation, the amplitudes for negative wave numbers can be found from the amplitudes of the positive wave numbers. In the x direction, the negative amplitude has to be equal to the positive one and, in the z direction, the negative amplitude has to have the same magnitude as the positive one but with the opposite sign. The amplitude for the positive wave numbers is calculated by inverting the boundary condition matrix in equation (20) and multiplying by the external excitation.

$$\begin{pmatrix} b_{1,1} & b_{1,2} & \cdots & b_{1,12} \\ b_{2,1} & b_{2,2} & & \\ \vdots & & \ddots & \vdots \\ b_{12,1} & & \cdots & b_{12,12} \end{pmatrix} \begin{pmatrix} A_{1+}^{lay1} \\ A_{1-}^{lay1} \\ A_{2+}^{lay1} \\ A_{2-}^{lay1} \\ A_{3+}^{lay1} \\ A_{3-}^{lay1} \\ A_{1+}^{lay2} \\ A_{1-}^{lay2} \\ A_{2+}^{lay2} \\ A_{2-}^{lay2} \\ A_{3+}^{lay2} \\ A_{3-}^{lay2} \end{pmatrix} = (\mathbf{P}_{ext}). \tag{20}$$

The radial response on the top surface of the upper layer can be calculated according to

$$\eta = -4j \sum_{m=1}^{\infty} \sum_{n=1}^{\infty} \eta_{m,n}^{lay2}(L_y) \cos(k_m x) \sin(k_n z), \tag{21}$$

where

$$\eta_{m,n}^{lay2}(L_y) = \sum_{o=1}^{3} [(A_{o+}^{lay2} \mathrm{e}^{-\mathrm{j}q_o L_y} + A_{o-}^{lay2} \mathrm{e}^{\mathrm{j}q_o L_y}) \mathbf{v}_o^{lay2}(\hat{\eta})]$$

and the tangential response may be calculated from

$$\xi = -4j \sum_{m=1}^{\infty} \sum_{n=1}^{\infty} \xi_{m,n}^{lay2}(L_y) \cos(k_m x) \sin(k_n z), \tag{22}$$

where

$$\xi_{m,n}^{lay2}(L_y) = \sum_{o=1}^{3} [(A_{o+}^{lay2} \mathrm{e}^{-\mathrm{j}q_o L_y} + A_{o-}^{lay2} \mathrm{e}^{\mathrm{j}q_o L_y}) \mathbf{v}_o^{lay2}(\hat{\xi})].$$

4.1. RESULTS COMPARED TO MEASUREMENTS

In order to verify the theoretical model, radial and tangential driving point mobilities were measured on a smooth 205/60/R15 tyre, i.e., a tyre without tread blocks. Figures 9 and 10 show the measurement set-ups used for the radial and the tangential measurements respectively.

The radial and tangential driving point mobilities were calculated using the wave approach method, including complex material parameters to take the damping into account. For both mobilities, a summation over wave numbers in the range up to 638/m was made, which corresponds to a shortest wavelength of 10 mm. An excitation area of 20 mm times 20 mm was chosen in the measurement. The material data used in the calculation are listed in Table 1, and Table 2 shows the loss factors used for the layers and the bedding springs.

Figure 11 shows the results for the measured driving point mobility in the radial direction compared to measurements.

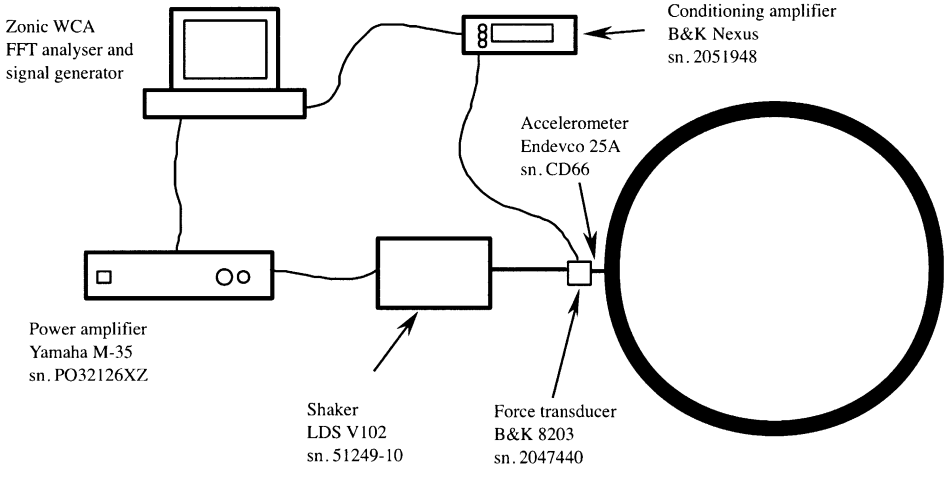

Figure 9. Measurement set-up for the radial driving point mobility measurements.

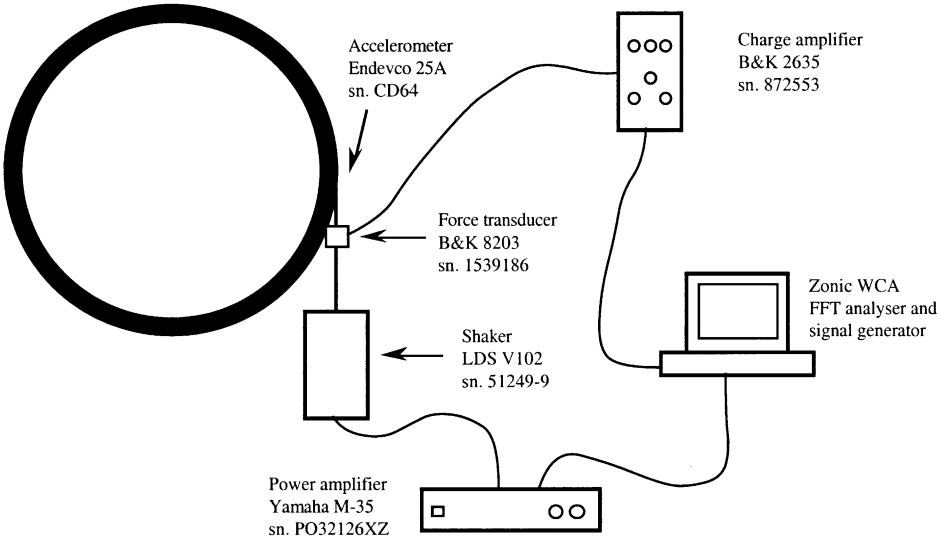

Figure 10. Measurement set-up for the tangential driving point mobility measurements.

TABLE 2

Values of loss factors for the tension, Young's modulus (E) in each layer and for the beddings

	Tension	*E*, layer 1	*E*, layer 2	Beddings
η	0·05	0·01	0·2	0·08

The discrepancy between measurements and calculations at low frequencies (below 400 Hz) is due to the curvature of the tyre being disregarded. Additionally, the resonance frequencies of the modes in the width direction are different for the calculation model and the real tyre. In the calculation model the stiffness is equal in both the x direction and the

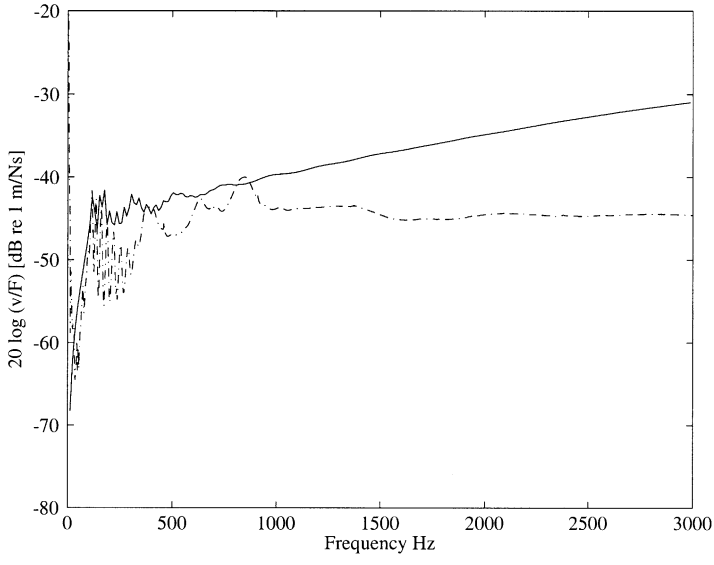

Figure 11. Calculated and measured radial driving point mobilities on the tyre. ———, calculation; · – · – · –, measurement.

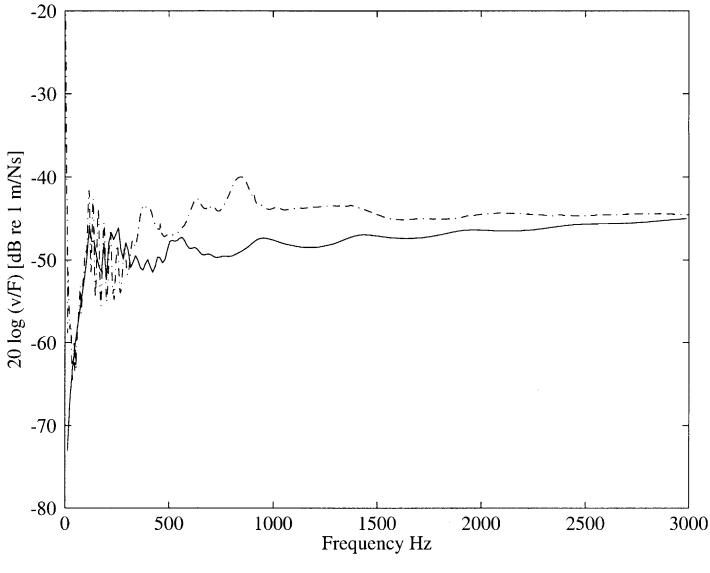

Figure 12. Calculated and measured radial driving point mobilities for stiff tread rubber show the effect of local stiffness. Young's modulus of tread rubber is 100 MPa. ———, calculation; · – · – · –, measurement.

z direction, while for a real tyre the stiffness varies in the different directions. Furthermore, the rim is considered as clamped in the calculation, which is hard to achieve in a real measurement situation.

At higher frequencies the calculated mobility is increasing with higher frequency, while the measured one is almost constant. The reason for the rise in the calculated curve is the local stiffness of the tread surface, due to a too low value of the shear modulus in the upper tread layer. Figure 12 shows the calculated radial point mobility compared to the

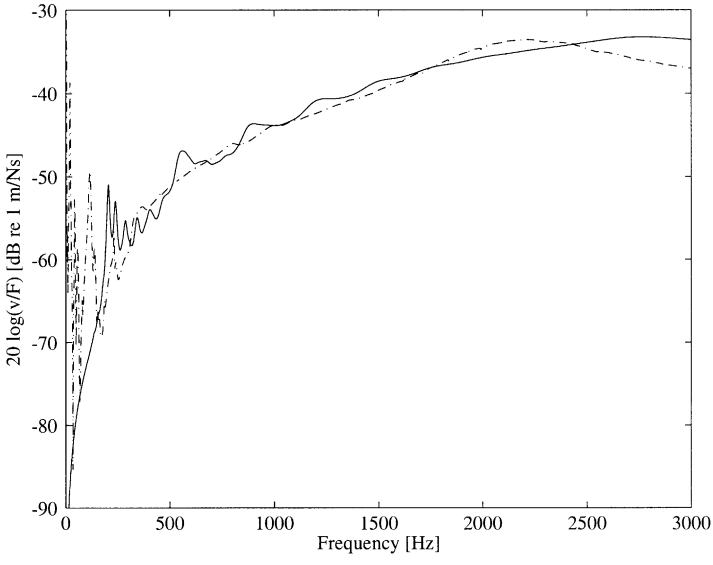

Figure 13. Calculated and measured tangential driving point mobilities on the tyre. ———, calculation; ·–·–·–, measurement.

measurements when the stiffness in the upper tread layer is increased from 20 to 100 MPa. As can be seen from the figure, the agreement is much better for the radial mobility in this case. However, for the tangential driving point mobility, the agreement with the measurement is poorer for this material combination.

Figure 13 shows the measured tangential driving point mobility compared to the calculated one. The agreement for this mobility is better than the radial one. The first resonance in the measurement corresponds to a rotation mode where the complete tyre rotates back and forth against the rim as a rigid body mode. This mode is not included in the calculation, which explains the discrepancy at low frequencies. The measurements also indicate that the damping is higher in the real tyre than that used in the calculation. The peaks are smoother and less visible in the measurements than in the calculations.

To achieve a better agreement the material parameters have to be adapted to measurements on real tyres. The largest source of uncertainty in the calculation is the material data for the two-layer model. The data found in the literature are often given as an average value of the tyre cross-section, e.g., bending stiffness and density. In the suggested model, the material data have to be given to each layer individually. Some of the parameters are simple to obtain like, for instance, the thickness, but most data are difficult to establish or measure, especially with respect to the complex structure of the steel layers.

5. CONCLUSIONS

To include the tangential contact forces between tyre and road in the existing tyre/road noise simulation model a description of the tangential motion of the tyre belt is needed. The tyre model proposed in this study is able to predict both radial and tangential responses of the tyre. At high frequencies the internal structure of the tyre increases in importance because the wavelength is no longer short compared to the thickness of the tyre.

The two-layer model can be used to study waves propagating along the tyre. Three wave types are found to be important in the frequency range of interest (up to 3 kHz): a membrane-bending wave, a longitudinal wave and an in-plane wave. The results of the dispersion relaions show good qualitative agreement both with other models and with measurements on real tyres. However, to achieve good quantitative agreement, the correct choice of the material data for each individual layers is required and will be a subject of future work.

The radial and tangential driving point mobilities of the tyre can be calculated using a wave approach.

One crucial point in the two-layer model is the material parameters. Often only average material data are given in the literature. To get a good agreement between calculations and measurements requires better defined material data for the individual layers.

ACKNOWLEDGMENT

This work has been financially supported by the Swedish Research Council for Engineering Sciences (TFR).

REFERENCES

1. D. STANNERS and P. BOURDEAU (editors) 1995 *Europe's Environment*. Copenhagen: European Environment Agency.
2. U. SANDBERG (editor) 1995 *Noise/News International* **6**, 85–113. The effects of regulations on road vehicle noise. [Report by the International Institute of Noise Control Engineering Working Party.]
3. J. A. EJSMONT 1997 *Proceedings of the* 2*nd International Seminar TIRE/ROAD NOISE*, *Gdansk*, *Poland*. Tire/road noise generating mechanisms and possible ways of their reduction.
4. D. RONNEBERGER 1989 *Tagungsbericht Workshop on Rolling Noise Generation*, *Berlin*. Towards quantitative prediction of tire road noise.
5. W. KROPP 1992 *Thesis*, *Fortschritt-Berichte* Reihe 11, Nr 166. Düsseldorf: VDI-Verlad. Ein Modell zur Beschreibung des Rollgeräusches eines unprofilierten Gürtelreifens auf rauher Straßenoberfläche.
6. F. BÖHM 1966 *Ingenieur Archiv* **35**, 82–101. Mechanik des Gürtely-reifens.
7. H. B. PACEJKA 1971 in *Mechanics of Pneumatic Tyres*, *Monograph* 122. (S.K. Clark, editor) Washington, DC: National Bureau of Standards. The tire as a vehicle component.
8. H. B. PACEJKA 1972 *Vehicle System Dynamics* **1**, 37–66. Analysis of the dynamic response of a rolling string-type tire model to lateral wheel-plane vibrations.
9. J. PADOVAN 1976 *Tire Science and Technology*, *TSTCA* **4**, 133–246. On viscoelasticity and standing waves in tires.
10. Y. B. CHANG, T. Y. YANG and W. SOEDEL 1984 *Journal of Sound and Vibration* **96**, 1–11. Dynamic analysis of a radial tirew by finite elements and modal expansion.
11. T. L. RICHARDS 1990 *Journal of Sound and Vibration* **149**, 235–243. Finite element analysis of structural–acoustic coupling in tyres.
12. E. J. NI, D. S. SNYDER, G. F. WALTON, N. E. MALLARD, G. E. BARRON, J. T. BROWELL and B. N. ALJUNDI 1997 *Tire Science and Technology*, *TSTCA* **25**, 29–42. Radiation noise from tire/wheel vibration.
13. W. KROPP 1989 *Applied Acoustics* **26**, 181–192. Structure-borne sound on a smooth tyre.
14. M. UEBLER 1996 *Ph. D. thesis*, *TU Berlin*, *Berlin*. Modell zur Berechnung der hochfrequencten Schwingungen eines profillosen stehenden Reifens und dessen Schallabstrahlung.
15. R. J. PINNINGTON and A. R. BRISCOE 1999 Accepted for publication in *Journal of Sound and Vibration*. A wave model for a pneumatic tyre belt.
16. M. HECKL 1990 *Acustica* **72**, 189–196. Einfache Anvendung des Hamiltonschen Prinzips bei Körperschallproblemen.
17. L. CREMER and M. HECKL 1996 *Körperschall*. Berlin: Springer-Verlag; second edition.

18. V. V. BOLOTIN 1963 *Non-conservative Problems of the Theory of Elastic Stability*. New York: The Macmillan Company.
19. R. D. COOK, D. S. MALKUS and M. E. PLESHA 1989 *Concepts and Applications of Finite Element Analysis*. New York: John Wiley & Sons; third edition.
20. J. D. ACHENBACH 1973 *Wave Propagation in Elastic Solids*. Amsterdam: North-Holland.
21. M. J. S. LOWE 1995 *IEEE Transactions on Ultrasonics, Ferroelectrics and Frequency Control* **42**, 525–542. Matrix techniques for modelling ultrasonic waves in multilayered media.
22. M. HECKL 1986 *Wear* **113**, 157–170. Tyre noise generation.
23. H. JOHANSSON *M.Sc. Thesis and Personal Communication, Chalmers University of Technology, Götenborg*. Application of the tyre noise simulation model.